Journal of Asian Earth Sciences 155 (2018) 188–197

Contents lists available at ScienceDirect

Journal of Asian Earth Sciences

journal homepage: www.elsevier.com/locate/jseaes

High resolution luminescence chronology for Xiashu Loess deposits of Southeastern China

Shuangwen Yi[a,*], Xusheng Li[a], Zhiyong Han[a], Huayu Lu[a], Jinfeng Liu[b], Jiang Wu[a]

[a] School of Geography and Ocean Science, Nanjing University, Jiangsu Collaborative Innovation Center for Climate Change, Nanjing 210023, China
[b] State Key Laboratory of Earthquake Dynamics, Institute of Geology, China Earthquake Administration, Beijing 100029, China

ARTICLE INFO

Keywords:
Southeastern China
Loess
Quartz OSL
Post-IR IRSL
Luminescence dating

ABSTRACT

Loess deposits in Xiashu are representative of such deposits in Southeastern China that are mainly distributed in the middle and lower reaches of the Yangtze River valley. These loess-paleosol sequences provide a key archive of past climate change in humid, subtropical regions. However, the ages of the sequences are not well constrained. In this study, the standard quartz single-aliquot regenerative (SAR) dose optically stimulated luminescence (OSL) and K-feldspar post-infrared infrared stimulated luminescence (post-IR IRSL; $pIRIR_{290}$) methods are used to date two loess sequences in Nanjing region. Our results show that quartz SAR OSL and K-feldspar $pIRIR_{290}$ ages are more or less indistinguishable from one another up to ~50 ka. Beyond this age, the K-feldspar pIRIR ages increased systematically with deposition depth, agreeing well with the expected ages as far as ~200 ka. On the basis of a fully independently-dated timescale, we are therefore able to propose, for the first time, a new age model for the Xiashu Loess deposits accumulated since the penultimate interglacial period. Using our newly obtained luminescence dating ages, we observe a marked difference between the loess accumulation rates in the two sequences, potentially forced by regional depositional processes and loess preservation.

1. Introduction

The loess-paleosol sequences of the Chinese Loess Plateau (CLP) provide significant information about past climatic and environmental changes which occurred during glacial-interglacial cycles (Liu, 1985; Liu and Ding, 1998; Sun et al., 1998; Sun and Ding, 1998; An et al., 2015). They are also regarded as an excellent terrestrial archive that can be used to understand global paleoclimatic change because of the close correlation between these loess-paleosol sequences and the marine oxygen isotopic record.

The loess deposits in the middle and lower reaches of the Yangtze River, Southeastern China, forming part of the loess deposits which have accumulated outside the CLP (Fig. 1), record the southeasterly advance of dust activity and a strengthening East Asian Winter Monsoon (EAWM) (Liu, 1985; Yang, 1991; Pan et al., 1995; Xia et al., 1999; Jiang et al., 1997; Lu et al., 2010). These eolian silt deposits represent a vital archive of paleoclimatic change in a humid, subtropical climatic region. Such eolian deposits were first identified in Xiashu Town, southern Jiangsu Province, and were consequently defined as the Xiashu Loess (Li and Fang, 1993). Numerous studies of the grain size characteristics of these loess deposits (Li et al., 1997, 2001; Qiao et al., 2003; Liu and Deng, 2014), and their chemical weathering (Yang et al., 2001; Chen et al., 2008; Hong et al., 2010), environmental magnetism (Zhang et al., 2007; Qiao et al., 2003), isotopic composition (Li et al., 2007; Qiao et al., 2011; Hong et al., 2013; Liu et al., 2014) and provenance (Li et al.,1997, 2001; Hao et al., 2010; Wang et al., 2018) have been conducted in an attempt to reconstruct the subtropical Quaternary paleoenvironment. However, the ages of the sequences are not well constrained (Wu, 1985; Yang, 1991; Li et al., 1997, 2001; Qiao et al., 2003). Some studies have indicated that dust deposits had reached as far south as 30°N by ~150 ka (Liu, 1985; Pan et al., 1995; Xia et al., 1999). Other studies have suggested that the southeasterly advance of dust transportation and deposition as far as this region occurred later than ~100 ka (Jiang et al., 1997). Moreover, someone argued that the eolian dust reached this area during the Early-Middle Pleistocene (Yang, 1991). Such controversial has undoubtedly arisen from the uncertain dating results, even though multiple techniques such as magnetostratigraphic, electron spin resonance (ESR), U-series, thermoluminescence (TL) and radiocarbon (^{14}C) dating methods, have been performed (Wu, 1985; Li and Fang, 1993; Li et al., 1993; Huang et al., 1988; Lai et al., 2001, 2010a). The ^{14}C dating of carbonates in these loess deposits appears to indicate that the Xiashu Loess is more or less synchronous with the L_1 loess unit on the CLP which was formed during the last glaciation, and which corresponds to marine isotope stages

* Corresponding author.
E-mail address: ysw7563@nju.edu.cn (S. Yi).

https://doi.org/10.1016/j.jseaes.2017.11.027
Received 15 September 2017; Received in revised form 16 November 2017; Accepted 16 November 2017
Available online 20 November 2017
1367-9120/ © 2017 Elsevier Ltd. All rights reserved.

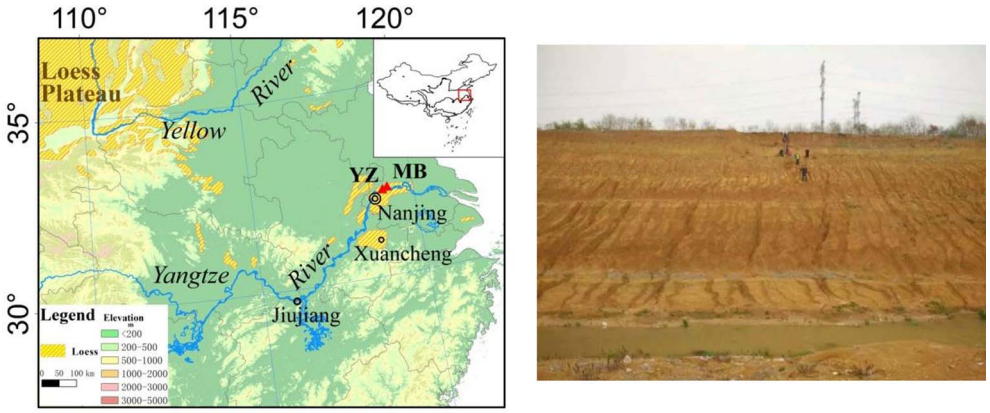

Fig. 1. Distribution of loess in Southeastern China, and location of study sites. The photograph is the MB loess-paleosol section.

(MIS) 2, 3 and 4, respectively (Wu, 1985). Moreover, the U-series dating of a fossilized deer horn, combined with the ESR dating, concluded that the Xiashu Loess was deposited between ~500–400 ka and 10 ka (Li and Fang, 1993; Li et al., 1993). By contrast, TL dating and palaeomagnetic stratigraphy analysis have both suggested that the Xiashu Loess was accumulated between ~730 and ~100 ka, with no L_1 loess layer present (Huang et al., 1988). Therefore, an accurate, high-resolution independently-constrained dating method for the Xiashu Loess deposits has become absolutely necessary.

Over the past several decades, the SAR dose-based OSL dating method (Wintle and Murray, 2006) has proven to be a particularly successful when dating the loess on the CLP (Stevens et al., 2006; Lu et al., 2006; Lu et al., 2007; Lu Y. et al., 2007; Buylaert et al., 2007; Lai, 2010b; Li and Li, 2011) and its adjacent regions in central and northern China (Lu et al., 2007, 2011; Sun et al., 2012; Yi et al., 2012, 2015, 2016). However, the application of the luminescence dating method to loess deposits in the Southeastern China remains limited. Seven ages for the loess at the Zhenjiang site south of Nanjing suggested that the post-IR blue-stimulated OSL method is more reliable than the IR signals extracted from polymineral samples (Watanuki and Tsukamoto, 2001; Watanuki et al., 2003). However, even after correction for laboratory fading, IR and post-IR blue-stimulated OSL signals underestimated the true age (Watanuki and Tsukamoto, 2001; Watanuki et al., 2003). Further, 17 fine grained (FG) IRSL ages from the Xujiachun Section near Nanjing suggested the first loess layer was formed during 72–14 ka, corresponding with the last glaciation (Lai et al., 2001). The IRSL- and ESR-dated ages, when compared with magnetic susceptibility values, suggested that the age of the lowermost layer of the Xiashu Loess is comparable with that of the L_5 loess observed at the Luochuan Section on the CLP; this finding indicated that loess had deposited in the middle and lower reaches of the Yantgze River by ~500 ka (Lai et al., 2001). Following on from this discovery, 13 loess samples from Nanjing and Jiujiang areas were dated, confirming that the first layer of the Xiashu Loess was deposited during the last glaciation (Lai et al., 2010a). However, quartz OSL dating is normally constrained to just the last ~50–70 ka because of its relatively minimal upper-limit doses (~200 Gy for loess deposits with a typical dose rate of 3–4 Gy/ka; Buylaert et al., 2007; Roberts, 2008); additionally, feldspar IRSL dating has been well-recognized as being prone to anomalous fading and therefore age underestimation is existed (Wintle, 1973; Spooner, 1994; Huntley and Lamothe, 2001). Recent advances have identified the low- or non-fading characteristics of IRSL signals measured at elevated temperatures after an IR stimulation (Thomsen et al., 2008; Jain and Ankjærgaard, 2011; Li and Li, 2011, 2012); this has led to the emergence of several so-called post-IR IRSL (pIRIR) techniques, including a two-step (Thomsen et al., 2008; Buylaert et al., 2009, 2012; Thiel et al., 2011) and a multi-step (Li and Li, 2011, 2012) elevated temperature pIRIR stimulation procedure. All these protocols have been proven to be particularly applicable to young (< 10 ka; Reimann and Tsukamoto, 2012; Fu and Li, 2013) and old (> 100 ka; Buylaert et al., 2012; Li and Li, 2011, 2012; Chen et al., 2015) samples. The pIRIR technique has thus become the preferred method for measuring feldspar equivalent doses (D_e), allowing the loess chronostratigraphy to be extended beyond the limits defined by quartz OSL dating.

This study aimed to test the applicability of the feldspar pIRIR method to the loess deposits in Southeastern China, and especially to the old loess deposits. We also aimed to obtain a reliable chronology for the loess-paleosol sequences in this study region. To achieve these goals, the luminescence characteristics of quartz SAR OSL and K-feldspar pIRIR signals ($pIRIR_{290}$) are investigated. The pIRIR signal is then further investigated in detail using a signal stability check, a dose recovery test, and long-timescale residual measurements. Finally, the quartz SAR OSL and $pIRIR_{290}$ ages are compared, and an absolute high-resolution dating chronology was developed for the loess deposits of Southeastern China.

2. Study area and samples

Nanjing and its surrounding areas such as Zhenjiang and Yizheng are covered by the typical Xiashu Loess (Fig. 1). The loess deposits exhibit a thickness of up to ~33 m, and as many as seven eolian loess-paleosol sequences are described. This region is dominated by the East Asian Summer Monsoon (EASM) from April to October, with a high mean annual precipitation (MAP; ~1000 mm).

The two study sites, i.e., Yizheng (YZ; 32.26°N, 119.06°E, 40 m asl) and Maba (MB; 32.31°N, 119.21°E, 29 m asl) are situated in the vicinity of Yizheng City, northeastern Nanjing (Fig. 1). The profile is characterized by clear brown-red loess and paleosol alternations (Fig. 1). The YZ Section has a thickness of ~18 m, whereas the MB Section has a thickness of ~23 m.

A total of 40 samples were collected from freshly excavated sections during fieldwork using light-tight steel cylinders (diameter ~5 cm, length ~25 cm), and were immediately sealed on-site to prevent light exposure and moisture loss prior to luminescence dating.

3. Methods

3.1. Sample preparation and experimental procedures

In the laboratory, all luminescence samples were handled under safe (subdued red) light conditions. The 2–5 cm of the material from the two outer ends of each tube was scraped away and kept for water content and dosimetry measurements. The 63–90 μm particles from the non-light-exposed inner part of each sample was extracted using standard procedures, including treatment with 30% hydrochloric acid and 30% hydrogen peroxide, in order to remove carbonates and organic matter, respectively. This procedure was followed by wet sieving. Afterwards, this fraction was cleaned with 10% hydrofluoric acid for 15 min to

Table 1
Quartz OSL and K-feldspar $pIRIR_{290}$ dose measurement protocols used in this study: (a) Quartz OSL protocol after Murray and Wintle (2003); and (b) Post-IR IRSL protocol modified from Thiel et al. (2011) and Buylaert et al. (2012). For the "natural" sample, $i = 0$ and $D_0 = 0$. The entire sequence is repeated for several regenerative doses, including zero and repeat doses.

Step	(a) SAR protocol	Observed	(b) $pIRIR_{290}$ protocol	Observed
1	Give regenerative dose, D_i		Give regenerative dose, D_i	
2	Preheat (160–300 °C, 10 s)		Preheat (320 °C, 60 s)	
3	OSL (125 °C, 40 s)	L_X	IRSL (50/200 °C, 200 s)	
4	Test dose		IRSL (290 °C, 200 s)	L_X
5	Cut-heat (160–300 °C)		Test dose	
6	OSL (125 °C, 40 s)	T_X	Preheat (320 °C, 60 s)	
7	OSL (280 °C, 40 s)		IRSL (50/200 °C, 200 s)	
8	Return to step 1		IRSL (290 °C, 200 s)	T_X
9			IRSL (325 °C, 200 s)	
10			Return to step 1	

remove any coatings and the outer α-irradiated layer, which was then rinsed in 10% hydrochloric acid for 20 min to remove any precipitated fluorides. K-rich feldspars were first separated from any quartz present using a heavy liquid (sodium heteropolytungstate, "LST Fastfloat"; density 2.58 $g{\cdot}cm^{-3}$). Subsequently, the remaining material was treated with 40% hydrofluoric acid for 40 min and rinsed using 10% hydrochloric acid for 40 min to obtain pure quartz grains. The purity of the quartz was further determined using the OSL-IR depletion ratio method (Duller, 2003). Samples with obvious IRSL signals were re-treated until the OSL-IR depletion ratio was uniform within 10%.

The quartz D_e value was determined using a standard SAR protocol (Table 1a; Murray and Wintle, 2000, 2003); this involved stimulating the OSL signal with blue LED diodes at 125 °C for 40 s. A step inserting an IR stimulation event at room temperature prior to OSL measurement was added to the last cycle in an attempt to monitor feldspar contamination (Duller, 2003). For K-feldspars, the D_e value was determined using the $pIRIR_{290}$ protocol (Table 1b; Thiel et al., 2011; Buylaert et al., 2012), which measures the luminescence as stimulated by infrared light at 290 °C after stimulation at 50 °C/200 °C (the choice of this temperature is discussed in the next section). This protocol is thought to be more stable than use of the standard IRSL signal (Thomsen et al., 2008; Jain and Ankjærgaard, 2011).

All luminescence measurements were made using a Risø TL/OSL reader (model DA-20C/D), fitted with blue LEDs (470 nm, ~80 $mW{\cdot}cm^{-2}$), infrared LEDs (870 nm, ~135 $mW{\cdot}cm^{-2}$) and an accurately-calibrated $^{90}Sr/^{90}Y$ beta source (Bøtter-Jensen et al., 2010). Quartz OSL signals were detected using a 7.5 mm-thick Schott U-340 glass filter, whereas feldspar (post-IR) IRSL readings were collected using a Corning 7–59 and Schott BG-39 glass filter combination.

3.2. Dose rates

Concentrations of uranium (U), thorium (Th) and potassium (K) were measured using the neutron activation analysis method. The *in situ* water content (*i.e.*, the moisture/dry mass ratio) was derived by weighing the sample before and after drying, before being assigned an absolute uncertainty of ± 5%. For the MB Section, the water content values were concentrated between 14% and 18%. For the YZ Section, the water content varied greatly; sometimes its value fell to < 5%, unrepresentative of loess. Thus, a mean water content value of 16.9% from the MB Section was used for age calculation. This value is similar to the values measured at other loess sites in the study region (Lai et al., 2010a; Watanuki et al., 2003). The cosmic dose rate was calculated using the formula proposed by Prescott and Hutton (1994). K-feldspar grains have an internal radioactivity due to the presence of ^{40}K within the crystal structure. Assumed K-feldspar dose rates with K and Rb concentrations of 12.5 ± 0.5% and 400 ± 100 ppm, respectively, were therefore used for internal dose rate calculations (Huntley and Baril, 1997). Moreover, small internal dose rate contributions to quartz and K-feldspar from U and Th were also included (at 0.030 ± 0.015 Gy/ka and 0.06 ± 0.03 Gy/ka, respectively; Mejdahl, 1987; Vandenberghe et al., 2008; Zhao and Li, 2005). Finally, the updated dose rate conversion factors proposed by Guérin et al. (2011) were used to convert elemental concentrations into an annual dose rate. The dosimetry data for all samples are summarized in Table 2.

4. Luminescence characteristics

4.1. Quartz OSL

During quartz D_e determination, pure quartz grains were mounted as large (~8 mm) aliquots on stainless steel discs prior to the OSL signal being derived through early background subtraction (i.e., the first 0.16 s minus any background signals from the 0.16–0.32 s interval) in order to minimize the influence of slow and medium components (Cunningham and Wallinga, 2010). Dose response curves (DRC) were fitted using the single saturating exponential described in the Analyst program, version 4.31.7 (Duller, 2015). Typical DRC and OSL decay curves (inset) are shown in Fig. 2a and b. Blue-light stimulated OSL signals rapidly decreased during the first second of stimulation, indicating that the signal is dominated by a fast component (Singarayer and Bailey, 2003).

Before D_e determination, a series of pretests, including the preheat plateau and dose recovery tests, was performed to obtain conditions suitable for accurate and reliable measurements to be taken. The preheat plateau was carried out on Sample NJU1774. The preheat temperature was increased stepwise from 180 °C to 280 °C at 20 °C intervals, and three aliquots were measured for each set temperature. As shown in Fig. 2c, a D_e plateau was observed between 180 °C and 280 °C, with good recycling ratios (0.9–1.1) and low recuperation values (< 5%), suggesting that the D_e values were independent of preheat temperatures. The suitability of our adopted SAR protocol was further checked using a dose recovery test, a test which is regarded as the most stringent test for any SAR-based protocol (Murray, 1996; Wallinga et al., 2000; Murray and Wintle, 2003). 12 aliquots from Sample NJU1774 were bleached twice with blue LED light (with a 10 ks pause between each 100 s light exposure episode, at room temperature), and a known dose was then provided and measured using the SAR protocol. The dose recovery ratio (*i.e.*, the given dose to measured dose ratio) was derived from the preheat temperature of 260 °C (10 s) and cut-heat 220 °C preheat settings, uniformly consistent within an error of 1σ (NJU1774: 0.98 ± 0.01, $n = 12$). Moreover, the recycling ratio lay between 0.9 and 1.1, and the recuperation value was < 3%, demonstrating that the SAR protocol had successfully made any corrections to compensate for sensitivities encountered during measurement cycles. A preheat temperature of 260 °C (10 s) and a cut-heat temperature of 220 °C were therefore chosen for all D_e measurements.

Lai et al. (2010a) reported that the test-dose sensitivity was dose dependent and dropped significantly when the regeneration dose was > 300 Gy for the OSL loess samples from Nanjing. However, the reasons for this drop were unclear. Recently, luminescence dating work conducted loess samples from the Nihewan Basin in North China have shown that OSL dose recovery ratios can be uniformly consistent within an error of 1σ when the given doses for eolian loess samples are < 300 Gy. After this point, ratios were > 1 (Liu et al., 2016). We performed the same test for our samples, administered different doses (from 50 Gy to 400 Gy), and then measured the dose recovery ratios for Sample NJU1774. As shown in Fig. 2d, dose recovery ratios were within 10% of a uniform value (when the mean value was 0.97 ± 0.02, n = 9), when the given doses were < 200 Gy. Beyond this value, the dose recovery ratio was < 1 and decreased with regenerative doses. By contrast, the saturation ratios (i.e., the ratio of the sensitivity-corrected

Table 2
Quartz OSL and K-feldspar $pIRIR_{290}$ dating results for the YZ and MB loess sections. The absolute uncertainty for water content is ± 5%. $pIRIR_{290}$ D_e values have a residual dose of 4 ± 1 Gy subtracted from the measured value. (*n*) denotes the number of aliquots contributing to the D_e calculation ("*A*" = quartz and "*B*" = K-feldspar).

Lab No.	Sample No.	Depth (m)	U (ppm)	Th (ppm)	K (%)	Water content (%)	Quartz dose rate (Gy/ka)	$pIRIR_{290}$ dose rate (Gy/ka)	Quartz D_e (Gy)	$pIRIR_{290}$ D_e (Gy)	Aliquots (n) A/B	Quartz age (ka)	$pIRIR_{290}$ age (ka)
NJU-1774	YZ01-50	0.50	2.82 ± 0.10	15.10 ± 0.39	2.04 ± 0.06	16.9	3.50 ± 0.17	3.82 ± 0.17	94 ± 5	114 ± 2	11/20	27 ± 2	30 ± 2
NJU-2301	YZ-80	0.80	2.51 ± 0.10	14.40 ± 0.39	1.96 ± 0.06	16.9	3.32 ± 0.16	3.66 ± 0.16	106 ± 4	123 ± 5	10/3	32 ± 2	34 ± 2
NJU-2302	YZ-150	1.50	2.24 ± 0.09	14.20 ± 0.38	1.88 ± 0.06	16.9	3.17 ± 0.15	3.51 ± 0.16	155 ± 7	153 ± 8	10/3	49 ± 3	44 ± 3
NJU-2303	YZ-200	2.00	2.43 ± 0.09	14.20 ± 0.38	1.96 ± 0.06	16.9	3.26 ± 0.16	3.60 ± 0.16	159 ± 7	159 ± 6	5/3	49 ± 3	44 ± 3
NJU-1775	YZ02-235	2.35	2.32 ± 0.09	15.10 ± 0.39	1.94 ± 0.06	16.9	3.26 ± 0.16	3.59 ± 0.16	> 160	170 ± 6	16/4	> 49	47 ± 3
NJU-2304	YZ-300	3.00	2.65 ± 0.10	14.50 ± 0.39	1.95 ± 0.06	16.9	3.29 ± 0.16	3.63 ± 0.16	> 172	186 ± 8	9/3	> 52	51 ± 3
NJU-2305	YZ-360	3.60	2.45 ± 0.10	14.70 ± 0.40	1.93 ± 0.06	16.9	3.24 ± 0.16	3.58 ± 0.16	> 203	218 ± 6	13/3	> 63	61 ± 3
NJU-2306	YZ-450	4.50	2.47 ± 0.10	14.20 ± 0.38	1.91 ± 0.06	16.9	3.18 ± 0.16	3.52 ± 0.16	> 209	265 ± 9	6/3	> 66	75 ± 4
NJU-2307	YZ-500	5.00	2.63 ± 0.10	13.90 ± 0.38	1.78 ± 0.06	16.9	3.10 ± 0.16	3.44 ± 0.16	> 194	268 ± 11	6/3	> 63	78 ± 5
NJU-1776	YZ03-580	5.80	3.50 ± 0.12	15.20 ± 0.40	1.75 ± 0.06	16.9	3.26 ± 0.16	3.59 ± 0.17	> 198	298 ± 11	8/4	> 61	83 ± 5
NJU-2308	YZ-630	6.30	2.65 ± 0.10	14.50 ± 0.39	1.83 ± 0.06	16.9		3.47 ± 0.16		269 ± 9	0/3		77 ± 4
NJU-1777	YZ04-720	7.20	2.84 ± 0.11	14.20 ± 0.37	1.88 ± 0.06	16.9		3.51 ± 0.16		391 ± 6	0/4		111 ± 5
NJU-2309	YZ-780	7.80	2.82 ± 0.11	15.20 ± 0.40	1.84 ± 0.06	16.9		3.54 ± 0.16		430 ± 26	0/3		121 ± 9
NJU-2311	YZ-830	8.30	2.79 ± 0.11	14.80 ± 0.40	1.88 ± 0.06	16.9		3.54 ± 0.16		590 ± 11	0/5		166 ± 8
NJU-2312	YZ-900	9.00	3.26 ± 0.12	14.20 ± 0.38	1.76 ± 0.06	16.9		3.48 ± 0.16		565 ± 17	0/4		163 ± 9
NJU-2313	YZ-960	9.60	3.21 ± 0.12	14.40 ± 0.39	1.83 ± 0.06	16.9		3.54 ± 0.16		671 ± 20	0/4		190 ± 10
NJU-1778	YZ05-1050	10.50	3.01 ± 0.11	15.00 ± 0.39	1.78 ± 0.06	16.9		3.48 ± 0.16		717 ± 18	0/4		206 ± 11
NJU-1779	YZ06-1150	11.50	2.46 ± 0.10	14.20 ± 0.37	1.32 ± 0.05	16.9		2.92 ± 0.13		> 835	0/4		> 286
NJU-1780	YZ07-1545	15.45	2.87 ± 0.11	15.10 ± 0.39	1.56 ± 0.05	16.9		3.25 ± 0.15		> 1019	0/4		> 314
NJU-1781	YZ08-1565	15.65	3.06 ± 0.11	15.70 ± 0.41	1.46 ± 0.05	16.9		3.23 ± 0.15		> 1057	0/4		> 327
NJU-2281	MB-A-30	0.30	2.47 ± 0.10	14.30 ± 0.39	1.79 ± 0.06	18.2	3.16 ± 0.15	3.50 ± 0.15	88 ± 6	106 ± 2	12/3	28 ± 2	30 ± 1
NJU-2282	MB-A-55	0.55	2.38 ± 0.10	13.30 ± 0.36	1.75 ± 0.06	17.4	3.04 ± 0.15	3.38 ± 0.15	114 ± 7	104 ± 3	9/3	37 ± 3	31 ± 2
NJU-2283	MB-A-82	0.82	2.55 ± 0.10	13.70 ± 0.37	1.81 ± 0.06	18.4	3.10 ± 0.15	3.45 ± 0.15	126 ± 8	124 ± 4	13/8	41 ± 3	36 ± 2
NJU-2284	MB-A-110	1.10	2.30 ± 0.09	13.50 ± 0.36	1.81 ± 0.06	15.4	3.12 ± 0.15	3.46 ± 0.16	140 ± 3	160 ± 4	8/4	45 ± 3	46 ± 2
NJU-2285	MB-A-160	1.60	2.49 ± 0.10	14.10 ± 0.38	1.96 ± 0.06	14.5	3.35 ± 0.17	3.69 ± 0.17	> 150	169 ± 2	12/4	> 45	46 ± 2
NJU-2286	MB-A-210	2.10	2.58 ± 0.10	14.50 ± 0.39	1.90 ± 0.06	16.9	3.25 ± 0.16	3.59 ± 0.16	> 163	212 ± 5	12/4	> 50	59 ± 3
NJU-2287	MB-A-260	2.60	2.42 ± 0.09	14.90 ± 0.40	1.79 ± 0.06	17.2	3.13 ± 0.15	3.47 ± 0.16	> 155	235 ± 5	7/8	> 50	68 ± 3
NJU-2289	MB-A-410	4.10	2.69 ± 0.10	14.60 ± 0.39	1.63 ± 0.05	15.7		3.38 ± 0.15		293 ± 3	0/4		87 ± 4
NJU-2315	MB-A-470	4.70	2.78 ± 0.11	13.40 ± 0.36	1.50 ± 0.05	14.8		3.21 ± 0.15		315 ± 4	0/4		98 ± 5
NJU-2290	MB-A-540	5.40	3.36 ± 0.12	14.60 ± 0.39	1.79 ± 0.06	17.0		3.58 ± 0.16		441 ± 8	0/5		123 ± 6
NJU-2291	MB-A-680	6.80	3.06 ± 0.11	14.90 ± 0.40	2.07 ± 0.06	16.8		3.78 ± 0.17		449 ± 7	0/7		119 ± 6
NJU-2292	MB-A-770	7.70	2.77 ± 0.11	14.90 ± 0.40	1.88 ± 0.06	15.1		3.61 ± 0.17		529 ± 7	0/5		147 ± 7
NJU-2293	MB-B-0	8.90	2.56 ± 0.10	14.10 ± 0.38	1.99 ± 0.06	16.8		3.55 ± 0.16		564 ± 7	0/4		159 ± 8
NJU-2316	MB-B-110	10.00	2.66 ± 0.10	14.80 ± 0.40	1.92 ± 0.06	13.7		3.64 ± 0.17		478 ± 19	0/5		131 ± 8
NJU-2294	MB-B-215	11.05	2.62 ± 0.10	14.00 ± 0.38	1.92 ± 0.06	17.3		3.46 ± 0.16		544 ± 10	0/10		157 ± 8
NJU-2295	MB-B-320	12.10	2.66 ± 0.10	14.80 ± 0.40	1.60 ± 0.05	16.5		3.26 ± 0.15		546 ± 18	0/5		168 ± 10
NJU-2296	MB-B-410	13.00	2.68 ± 0.10	14.50 ± 0.39	1.79 ± 0.06	15.0		3.45 ± 0.16		706 ± 18	0/6		205 ± 11
NJU-2297	MB-B-640	14.85	2.95 ± 0.11	15.40 ± 0.40	1.78 ± 0.06	14.4		3.56 ± 0.17		799 ± 12	0/4		224 ± 11
NJU-2298	MB-C-170	16.90	2.55 ± 0.10	14.80 ± 0.40	1.51 ± 0.05	18.5		3.08 ± 0.14		783 ± 32	0/3		254 ± 16
NJU-2299	MB-C-390	19.15	2.92 ± 0.11	14.70 ± 0.40	1.46 ± 0.05	17.1		3.13 ± 0.14		> 968	0/6		> 309

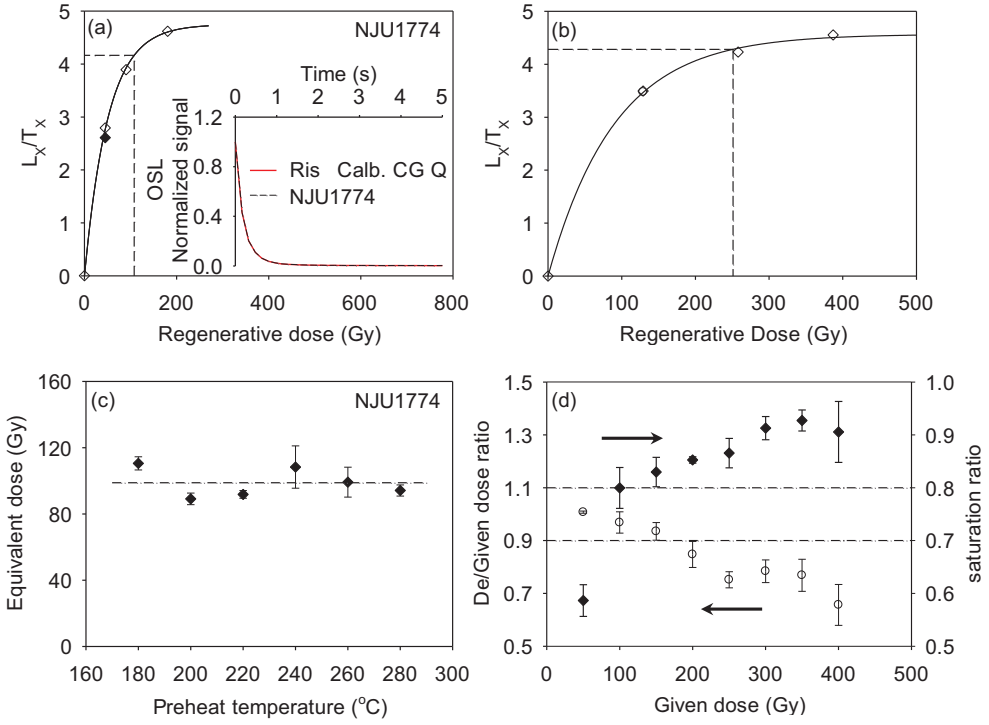

Fig. 2. Quartz luminescence characteristics. (a) and (b): Typical dose response curves for the aliquots of samples NJU1774 and NJU1776 (inset shows the natural decay curves); (c) Preheat plateau tests for Sample NJU1774. Three aliquots are measured at each temperature, with error bars representing one standard error. The dashed-dotted line represents the mean D_e value for the 180–280 °C interval; and (d) Results of the dose recovery test for OSL dating on Sample NJU1774, with the different doses provided. The dashed-dotted line represents a ± 10% deviation of the unity.

natural signal to the laboratory saturation level) increased. Meanwhile, for samples older than 200 Gy, the DRC appeared close to the saturation value (Fig. 2b), and the natural signals (L_N/T_N) of samples were approximately at, or exceeded, 85% of the maximum achievable value (i.e., $2D_0$ for a single saturating exponential, as defined by Wintle and Murray, 2006). We therefore deduced that the Xiashu Loess in the Nanjing area was consistent with that described in earlier studies, thereby suggesting that the upper limit of SAR-based quartz OSL dating lies at ~200 Gy in loess, and that any ages derived from these high doses were likely to have been underestimated (Buylaert et al., 2007; Lai, 2010b).

The calculated quartz OSL D_e values and ages are presented in Table 2. D_e values at the YZ Section ranged from 94 ± 5 Gy for the uppermost sample, to > 160 Gy; the corresponding ages were 27 ± 2 ka and > 50 ka, respectively. For the MB Section, D_e values ranged from 88 ± 6 Gy for the uppermost sample, to > 150 Gy; the corresponding ages were 28 ± 2 ka and > 50 ka, respectively.

4.2. K-feldspar $pIRIR_{290}$

During K-feldspar $pIRIR_{290}$ D_e determination, small (~2 mm) aliquots were placed on stainless-steel cups, and the first 2 s minus a background based on the last 50 s of the integrated signal was used for signal calculation. Representative K-feldspar $pIRIR_{290}$ DRC for Sample NJU1776 are presented in Fig. 3a. As shown in the figure, the K-feldspar $pIRIR_{290}$ DRC indicate a considerably extended dose range, suggesting an increased ability to date samples beyond the known quartz OSL limits.

The stability of the pIRIR signal has been deemed dependent on the first IR stimulation temperature and/or wavelength (Jain and Ankjærgaard, 2011; Li and Li, 2011, 2012). Buylaert et al. (2012) proposed an initial IR stimulation plateau test to identify whether a stable signal has, or has not, been reached. To do this, three aliquots were measured at each temperature prior to IR stimulation at 30 °C stepwise intervals between 50 °C and 260 °C. If the D_e values did not vary significantly over a certain temperature range, then the signal was taken to be independent of the first stimulation temperature, and therefore likely to be stable (Buylaert et al., 2012). As shown in Fig. 3b, the D_e value was insensitive to the first IR stimulation temperature, indicating that, for our samples, any initial stimulation temperature in the 50–260 °C range could be chosen. As a result, all doses were measured using the first IR stimulation temperature of 50 °C/200 °C (Table 1b).

The importance of a good dose recovery ratio for pIRIR dating has recently been reinforced (Li et al., 2014). However, difficulties in bleaching natural $pIRIR_{290}$ signals (Thomsen et al., 2008; Buylaert et al., 2012; Kars et al., 2014; Yi et al., 2016) are commonly recognized and sometimes lead to poor dose recovery ratios because of incorrect residual dose estimation (Stevens et al., 2011; Alexanderson and Murray, 2012). To overcome these potential complications, a dose recovery test can be performed by adding different β doses to young samples; the dose recovery ratio can then be calculated as the measured dose divided by the sum of the natural and given doses (Buylaert et al., 2011). In this study, a young sample (NJU2283) from the MB Section, with a $pIRIR_{290}$ D_e value of ~120 Gy, was chosen prior to being added to doses ranging from 0 Gy to ~800 Gy. In contrast, the test dose was kept constant at ~30% of the total measured dose (Yi et al., 2016). The dose recovery ratio was satisfactory up to ~700 Gy (Fig. 3c). For the YZ Section, the dose recovery ratio was 1.03 ± 0.04 (n = 3) from the uppermost sample (NJU1774, D_e value ~114 Gy). After this point, dose recovery ratios deviated from the uniform value.

Existing studies have shown that the residual dose for pIRIR signals can vary from a few Gy (< 2 Gy) to 10–20 Gy, or even > 30 Gy (Thiel et al., 2011; Stevens et al., 2011; Buylaert et al., 2011, 2012; Murray et al., 2012, 2014; Kars et al., 2014). The dose increased as a function of preheat and/or stimulation temperatures (Reimann et al., 2011; Fu et al., 2012) and also dose dependence, i.e., large residual doses were obtained from samples with large D_e values (Sohbati et al., 2012; Buylaert et al., 2012). Recent long-term laboratory bleaching experiments (> 80 days) on loess samples from Northeastern China have shown that a constant (or highly difficult to bleach) residual $pIRIR_{290}$ signal is reached after ~300 h; this corresponds to a dose of 6.2 ± 0.7 Gy (Yi et al., 2016). To investigate the degree to which our $pIRIR_{290}$ signal was bleachable, we repeated the experiment. A total of

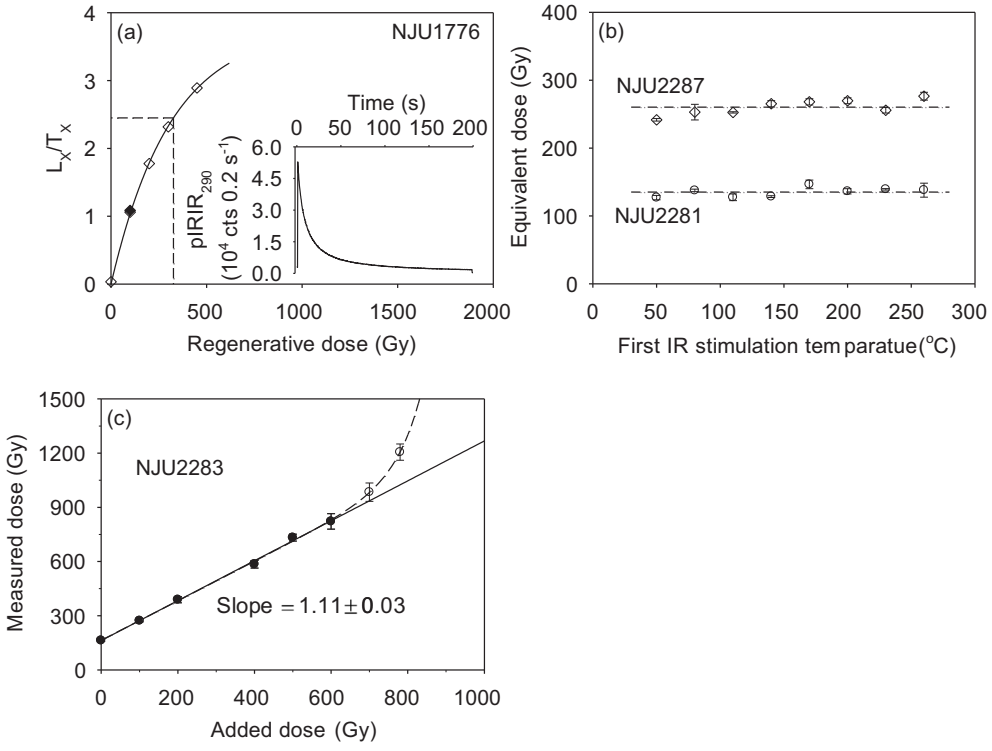

Fig. 3. K-feldspar $pIRIR_{290}$ luminescence characteristics: (a) Representative dose response curve for Sample NJU1776. The insets show the natural stimulation curves; (b) Dependence of D_e on the prior IR stimulation temperature for samples NJU2281 and 2287. Three aliquots were measured at each temperature, with error bars representing one standard error. The dashed-dotted line represents the mean D_e value for the 50–260 °C interval; and (c) Results of the dose recovery tests, showing measured *versus* added doses.

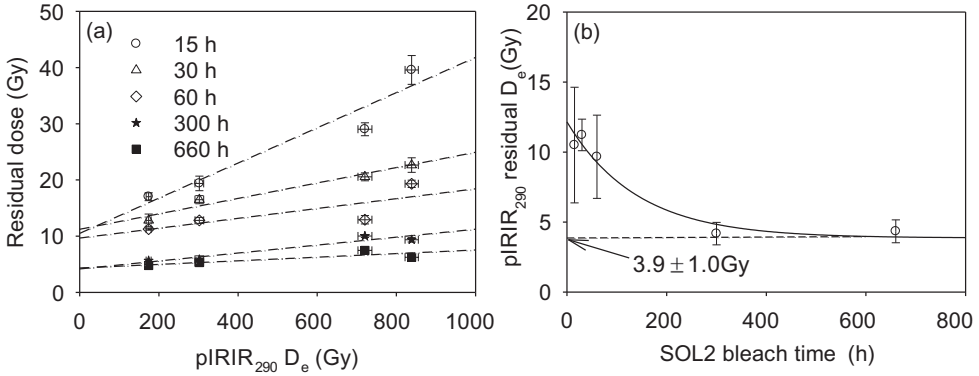

Fig. 4. Residual doses: (a) Mean residual dose obtained after different Hönle SOL2 solar simulator bleaching times as a function of the $pIRIR_{290}$ D_e value. Each point represents the mean residual dose of three aliquots *per* sample obtained after the given exposure times, and error bars represent one standard error; (b) Intercept of the linear fits with the *y*-axis from (a), as a function of exposure time.

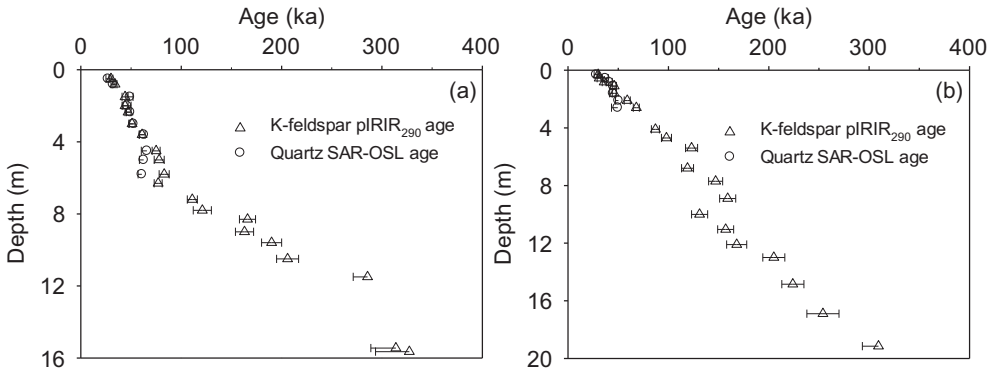

Fig. 5. Quartz OSL and K-feldspar $pIRIR_{290}$ ages for the: (a) YZ; and (b) MB sections. Open circles represent the quartz OSL ages; triangular circles represent the $pIRIR_{290}$ ages.

60 aliquots were extracted from four samples from the top, middle and bottom of the YZ Section (labeled NJU1775, NJU1776, NJU1778 and NJU1779); groups of three aliquots from each of these samples were then exposed in a Hönle SOL2 simulator at a lamp-to-sample distance of 80 cm over various periods (15 hr to 660 hr). Residual doses tended to increase with the D_e value (Fig. 4a), and the residual dose appeared consistent with the constant (or highly difficult to bleach) dose (corresponding to a dose of ~4 ± 1 Gy) after a bleaching period of ~300 h (Fig. 4b). In our view it is likely that these apparently constant difficult-to-bleach signals were present in these samples at the time of deposition. Accordingly, this value was subtracted from all $pIRIR_{290}$ D_e values before the final age calculation.

The resulting $pIRIR_{290}$ D_e values, with ages, are summarized in Table 2. D_e values ranged from 114 ± 2 Gy for the uppermost sample

to > 1057 Gy for the lowermost sample in the YZ Section; the corresponding ages were 30 ± 2 ka and > 327 ka, respectively. For the MB Section, D_e values ranged from 106 ± 2 Gy for the uppermost sample to > 968 Gy for the lowermost sample; the corresponding ages were 30 ± 1 ka and > 309 ka, respectively. By cross-referencing dose recovery ratios, we assumed that D_e values within ~700 Gy (the corresponding age being ~200 ka) were likely to be highly accurate.

5. Discussion

5.1. Chronology of the loess sequences

The quartz SAR-OSL and K-feldspar $pIRIR_{290}$ ages are shown in Fig. 5 and Table 2. Quartz OSL ages systematically increased with depth from ~30 ka to ~50 ka for both sections. Beyond this value, quartz ages increasingly underestimated depositional ages because of signal saturation (i.e., $2D_0$ criterion, Wintle and Murray, 2006). This finding is consistent with the ~50–70 ka upper limit of SAR-based quartz OSL dating for loess (Buylaert et al., 2007; Roberts, 2008). The K-feldspar $pIRIR_{290}$ ages also increased systematically from ~30 ka to ~200 ka, along with stratigraphic order. Quartz and feldspar ages generally agreed well with each other as far as ~50 ka for samples from the uppermost layer, and no detectable systematic deviation is found between quartz and feldspar methods within the 0–50 ka period (Fig. 6). Feldspar IRSL DRC values increased significantly to markedly high doses; this dating method exhibited the potential to extend the datable age range by a factor of 4–5 compared with quartz SAR-OSL dating (Thomsen et al., 2008; Li and Li, 2011; Thiel et al., 2011; Buylaert et al., 2012). The consistency between feldspar and quartz values in the low age range confirmed the reliability of old pIRIR ages when they become older than quartz ages. Furthermore, as shown in Fig. 7, good agreement amongst feldspar $pIRIR_{290}$ ages is observed, and expected results obtained, using the Bacon age-depth model (Blaauw, 2010; Blaauw and Christen, 2011). This finding also demonstrated that $pIRIR_{290}$ signals can be used to determine ages as old as ~200 ka. We therefore used $pIRIR_{290}$ data as our preferred ages in our analysis.

As shown in Figs. 5 and 6 and Table 2, the resultant quartz OSL and feldspar $pIRIR_{290}$ ages for the uppermost layers of both sections ranged from ~30 ka to 50 ka, indicating that the loess was deposited during the last glacial period, and that it can be taken as equivalent to the L_1 loess observed on the CLP (Liu, 1985; Lu Y. et al., 2007). Further, the K-feldspar pIRIR ages increased systematically from ~30 ka to > 200 ka, suggesting that loess was deposited in Southeastern China by ~200 ka, corresponding to MIS 7 (Lisiecki and Raymo, 2005). These results are consistent with the results from previous studies where the first loess layer of Xiashu Loess was deposited during the last glaciation (Lai et al., 2001). We have therefore, for the first time, proposed a high-resolution and fully independently-dated age control for loess deposition in this study region since ~200 ka.

5.2. Quartz and feldspar age comparison: insights into the loess deposition in Southeastern China

The daylight bleaching rate of feldspar IR signals is known to be much slower than that of quartz OSL signals, whereas the pIRIR signal is more slowly bleached than the IR_{50} signal (Thomsen et al., 2008; Buylaert et al., 2012; Murray et al., 2012). A method was therefore proposed to examine the bleaching situation in relation to sedimentary deposition by comparing different luminescence signals with different sensitivities to daylight (Murray et al., 2012; Buylaert et al., 2013). As shown in Figs. 6 and 7, a good agreement is observed between the ages derived from quartz OSL and K-feldspar $pIRIR_{290}$ signals for samples from both loess sections, within known quartz SAR-OSL dating limits. These findings confirm that the quartz OSL signals were fully bleached prior to loess deposition, and that the $pIRIR_{290}$ signals were bleached much more slowly than the quartz OSL signals. For all the measured samples, the IR_{50} to $pIRIR_{290}$ dose ratios all lay on a smooth curve below a gradient value of 1 (Fig. 8), as would have been expected from samples for which both signals were well-bleached at deposition, but for which the IR_{50} signal was significantly unstable compared with the $pIRIR_{290}$ signal (Buylaert et al., 2013). More recent evidence derived from provenance tracing studies has shown that loess materials which are derived from FG floodplain material found in local river valleys or lakebeds, and exposed during glacial periods, have played an important role as the source of Xiashu Loess (Wu et al., 1992; Qiao et al., 2003, 2011; Hao et al., 2010; Hong et al., 2013; Wang et al., 2018). Our results suggested that the eolian dust experienced prolonged and ideal light exposure before its final deposition. Based on our preferred ages (< 50 ka for quartz and feldspar; > 50 ka for feldspar only), we inferred that loess accumulation rates varied at the two sections, especially at ~100 ka (Fig. 9). For example, there was a distinct change in loess accumulation evident in the YZ Section at ~100 ka, when there appears to have been a depositional hiatus (Fig. 5a, 7a). By contrast, the K-feldspar pIRIR ages of the MB Section increased systematically from ~30 ka to > 200 ka with no distinct hiatus, and little variation in the loess accumulation rate (Fig. 5b, 7b). Loess accumulations at both sites show similar tendencies before ~100 ka in spite of some perceptible discrepancies. After this time, discrepancies become more pronounced, even showing an inverse trend (Fig. 9). This finding is very different from the loess deposition patterns observed on the CLP (Liu, 1985; Lu et al., 2010), although our two study sites are situated in the same region. This might be explained by the complexity of the loess' depositional process, which is principally controlled by the abundance or otherwise of its material sources, the relative strength of any transportation process, and the geographical suitability of any potential sedimentary environment. Moreover, the accumulation rate is related to surface processes and any climate change experienced by the source and the sedimentary area (Lu et al., 2010). Our study area is characterized by a hilly (low altitude) topography and a high-precipitation (~1000 mm) summer monsoonal climate, potentially influencing the

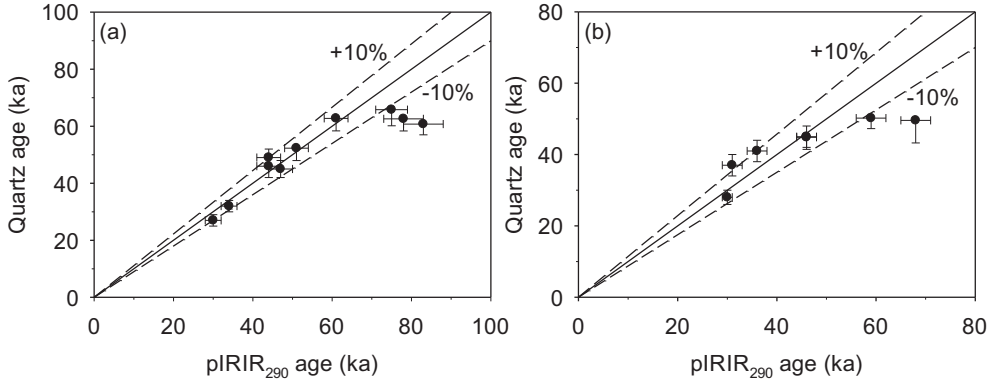

Fig. 6. Comparison of quartz OSL and K-feldspar $pIRIR_{290}$ ages for the uppermost loess layer of the: (a) YZ; and (b) MB sections. The $pIRIR_{290}$ ages have a subtracted residual dose of 4 ± 1 Gy. The solid line is the 1:1 line, and the dashed lines show the ± 10% deviation.

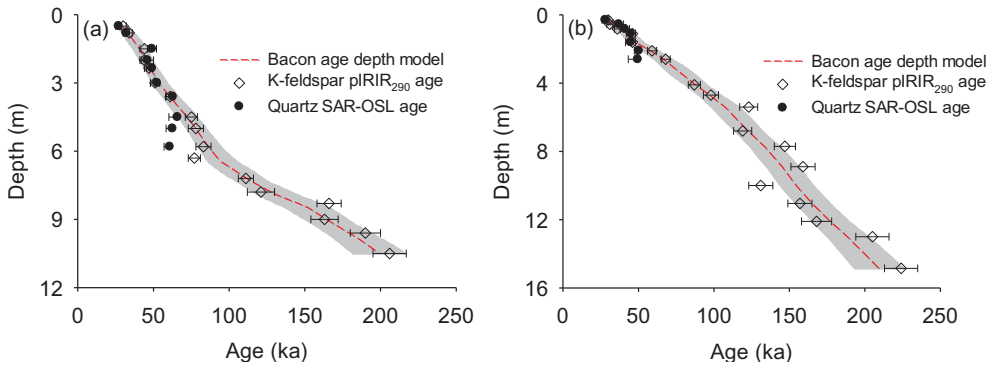

Fig. 7. Reconstructed Bacon age-depth model (red dashed line) derived from K-feldspar $pIRIR_{290}$ ages for the: (a) YZ; and (b) MB sections. Gray shading indicates the 95% probability intervals of the age-depth models.

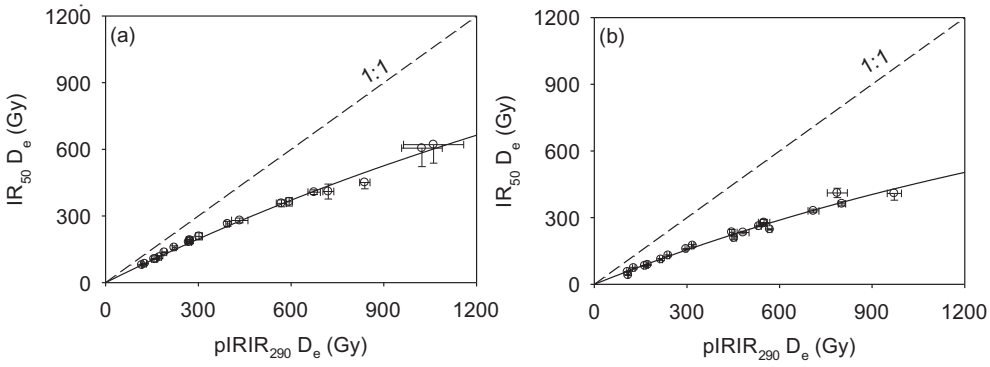

Fig. 8. Comparison of D_e values derived from feldspar IR_{50} and $pIRIR_{290}$ signals for all measured samples from the: (a) YZ; and (b) MB sections. The dashed grey line is the 1:1 line, and the solid line shows the fit of $pIRIR_{290}$ and IR_{50} D_e values with a single exponential function.

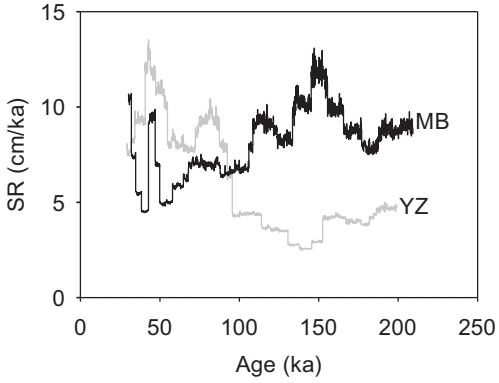

Fig. 9. Depositional rates for loess for the YZ and MB sections, based on high-resolution luminescence dating chronologies.

manner and degree of any transportation of eolian dust from the source region, as well as any loess deposition. However, there are other potential controls which require further investigation. Our results have confirmed that an accurate and precise age model is critical when using loess deposition to reconstruct paleoclimatic and environmental changes in Southeastern China.

6. Conclusions

High-resolution luminescence dating using quartz OSL and K-feldspar techniques is conducted on the loess deposited in Southeastern China. Quartz dating is sensitive, fast component-dominated, and exhibited excellent luminescence characteristics. The measured D_e values for feldspar $pIRIR_{290}$ do not vary significantly for the initial IR stimulation temperatures between 50 °C and 260 °C; the dose recovery ratio is uniformly consistent for doses up to ~700 Gy when the test dose is ~30% of the total dose. For our samples, there is a constant (or highly difficult to bleach) residual value of ~4 ± 1 Gy evident in $pIRIR_{290}$ signals, even after ~300 h of SOL2 bleach time.

Quartz OSL and K-feldspar $pIRIR_{290}$ ages appear indistinguishable up to ~50 ka. For old sediments, quartz OSL increasingly underestimates the depositional age because of signal saturation. By contrast, K-feldspar $pIRIR_{290}$ ages increase systematically with depth and are in satisfactory agreement with the expected ages, demonstrating that $pIRIR_{290}$ signals can be used to determine ages as old as ~200 ka for loess deposit in the subtropical, monsoonal area of Southeastern China.

On the basis of our calculations on independently-controlled dating methods, the loess accumulation rates have an apparent difference between the two loess deposition sequences, possibly influenced by the local environment *via* different sedimentary sources, preservation and topographical processes. Our investigation proves that an accurate, precise age model is critical for fully understanding paleoclimatic and environmental changes recorded by the Xiashu Loess.

Acknowledgements

We would like to thank Professor Sun Jimin for inviting us to write this paper. We are also grateful to Mr. Yuan Xiaokang and Mr. Yang Chuanbin for their assistance during the fieldwork and laboratory analyses. This research was supported by the National Natural Science Foundation of China (grant nos. 41371203,41690111, 41571188) and the Global Change Program of the Ministry of Science and Technology of China (grant nos. 2016YFA0600503 and 2016YFE010950).

References

Alexanderson, H., Murray, A.S., 2012. Luminescence signals from modern sediments in a glaciated bay, NW Svalbard. Quat. Geochronol. 10, 250–256.
An, Z.S., Wu, G.X., Li, J.P., Sun, Y.B., Liu, Y.M., Zhou, W.J., Cai, Y.J., Duan, A.M., Li, L., Mao, J.Y., Cheng, H., Shi, Z.G., Tan, L.C., Yan, H., Ao, H., Chang, H., Feng, J., 2015. Global monsoon dynamics and climate change. Annu. Rev. Earth Planet. Sci. 43, 29–77.
Blaauw, M., 2010. Methods and code for classical age-modelling of radiocarbon

sequences. Quat. Geochronol. 5, 512–518.
Blaauw, M., Christen, J.A., 2011. Flexible paleoclimate age-depth models using an autoregressive gamma process. Bayesian Anal. 6, 457–474.
Bøtter-Jensen, L., Thomsen, K.J., Jain, M., 2010. Review of optically stimulated luminescence (OSL) instrumental developments for retrospective dosimetry. Radiat. Meas. 45, 253–257.
Buylaert, J.P., Vandenberghe, D., Murray, A.S., Huot, S., De Corte, F., Van den haute, P., 2007. Luminescence dating of old (> 70 ka) Chinese loess: a comparison of single-aliquot OSL and IRSL techniques. Quat. Geochronol. 5, 9–14.
Buylaert, J.P., Murray, A.S., Thomsen, K.J., Jain, M., 2009. Testing the potential of an elevated temperature IRSL signal from Kfeldspar. Radiat. Meas. 44, 560–565.
Buylaert, J.P., Thiel, C., Murray, A.S., Vandenberghe, D., Yi, S.W., Lu, H.Y., 2011. IRSL and post IR-IRSL residual doses recorded in modern dust samples from the Chinese loess plateau. Geochronometria 38, 432–440.
Buylaert, J.P., Jain, M., Murray, A.S., Thomsen, K.J., Thiel, C., Sohbati, R., 2012. A robust feldspar luminescence dating method for Middle and Late Pleistocene sediments. Boreas 41, 435–451.
Buylaert, J.P., Murray, A.S., Gebhardt, A.C., Sohbati, R., Ohlendorf, C., Thiel, C., Wastegård, S., Zolitschka, B., The PASADO Science Team, 2013. Luminescence dating of the PASADO core 5022–1D from Laguna Potrok Aike (Argentina) using IRSL signals from feldspar. Quat. Sci. Rev. 71, 70–80.
Chen, Y.W., Li, S.H., Li, B., Hao, Q.Z., Sun, J.M., 2015. Maximum age limitation in luminescence dating of Chinese loess using the multiple-aliquot MET-pIRIR signals from K-feldspar. Quat. Geochronol. 20, 207–212.
Chen, Y.Y., Li, X.S., Han, Z.Y., Yang, S.Y., Wang, Y.B., Yang, D.Y., 2008. Chemical weathering intensity and element migration features of the Xiashu loess profile in Zhenjiang, Jiangsu Province. J. Georg. Sci. 18, 341–352.
Cunningham, A.C., Wallinga, J., 2010. Selection of integration time intervals for quartz OSL decay curves. Quat. Geochronol. 5, 657–666.
Duller, G.A.T., 2015. The Analyst software package for luminescence data: overview and recent improvements. Ancient TL 33, 35–42.
Duller, G.A.T., 2003. Distinguishing quartz and feldspar in single grain luminescence measurements. Radiat. Meas. 37, 161–165.
Fu, X., Li, B., Li, S.H., 2012. Testing a multi-step post-IR IRSL dating method using polymineral fine grains from Chinese loess. Quat. Geochronol. 10, 8–15.
Fu, X., Li, S.H., 2013. A modified multi-elevated-temperature post-IR IRSL protocol for dating Holocene sediments using K-feldspar. Quat. Geochronol. 17, 44–54.
Guérin, G., Mercier, N., Adamiec, C., 2011. Dose-rate conversion factors: update. Ancient TL 29, 5–8.
Hao, Q.Z., Guo, Z.T., Qiao, Y.S., Xu, B., Oldfield, F., 2010. Geochemical evidence for the provenance of middle Pleistocene loess deposits in southern China. Quatern. Sci. Rev. 29, 3317–3326.
Hong, H.L., Gu, Y.S., Li, R.B., Gu, Y.S., Wu, Y.B., Yin, K., Li, Z.H., 2010. Clay mineralogy and geochemistry and their palaeoclimatic interpretation of the Pleistocene deposits in the Xuancheng Section, South China. J. Quat. Sci. 25, 662–674.
Hong, H.L., Wang, C.W., Zeng, K.F., Gu, Y.S., Wu, Y.B., Yin, K., Li, Z.H., 2013. Geochemical constraints on provenance of the mid-Pleistocene red earth sediments in subtropical China. Sediment. Geol. 290, 97–108.
Huang, J.N., Fang, J.Y., Shao, J.J., Yang, D.Y., 1988. Study on the chronology of Xiashu loess in Nanjing area. Geol. Rev. 34, 241–246 (in Chinese with English abstract).
Huntley, D.J., Baril, M.R., 1997. The K content of the K-feldspars being measured in optical dating or in thermoluminescence dating. Ancient TL 15, 11–13.
Huntley, D.J., Lamothe, M., 2001. Ubiquity of anomalous fading in K-feldspars and the measurement and correction for it in optical dating. Can. J. Earth Sci. 38, 1093–1106.
Jain, M., Ankjærgaard, C., 2011. Towards a non-fading signal in feldspar: insight into charge transport and tunnelling from time-resolved optically stimulated luminescence. Radiat. Meas. 46, 292–309.
Jiang, F.C., Wu, X.H., Xiao, H.G., Zhao, Z.Z., Wang, S.M., Xue, B., 1997. Age of the vermiculated red soil in Jiujiang area, south China. J. Geome. 4, 27–32 (in Chinese with English abstract).
Kars, R.H., Reimann, T., Ankjærgaard, C., Wallinga, J., 2014. Bleaching of the post-IR IRSL signal: new insights for feldspar luminescence dating. Boreas 37, 441–449.
Lai, Z.P., Zhou, J., Xia, Y.F., Zhang, J.Z., Chen, J., 2001. Luminescence dating of Xiashu loess in Nanjing. Prog. Nat. Sci. 11, 203–207 (in Chinese with English abstract).
Lai, Z.P., Zhang, W.G., Chen, X., Jia, Y.L., Liu, X.J., Fan, Q.S., Long, H., 2010a. OSL chronology of loess deposits in eastern China and its implications for East Asian monsoon history. Quat. Geochronol. 5, 154–158.
Lai, Z.P., 2010b. Chronology and the upper dating limit for loess samples from Luochuan section in the Chinese Loess Plateau using quartz OSL SAR protocol. J. Asian Earth Sci. 37, 176–185.
Li, B., Jacobs, Z., Roberts, R.G., Li, S.H., 2014. Review and assessment of the potential of post-IR IRSL dating methods to circumvent the problem of anomalous fading in feldspar luminescence. Geochronometria 41, 178–201.
Li, B., Li, S.H., 2011. Luminescence dating of K-feldspar from sediments: a protocol without anomalous fading correction. Quat. Geochronol. 6, 468–479.
Li, B., Li, S.H., 2012. Luminescence dating of Chinese loess beyond 130 ka using the non-fading signal from K-feldspar. Quat. Geochronol. 10, 24–231.
Li, F.C., Jin, Z.D., Xie, C.R., Feng, J.Y., Wang, L.B., Yang, Y.Z., 2007. Roles of sorting and chemical weathering in the geochemistry and magnetic susceptibility of the Xiashu Loess, East China. J. Asian Earth Sci. 29, 813–822.
Li, L.W., Fang, Y.S., 1993. Study on the Xiashu loess in Nanjing area. J. Nanjing Normal Univ. 16 (Suppl.), 3–21 (in Chinese with English abstract).
Li, X.G., He, J.H., Li, D.S., Li, L.W., 1993. The primitive application of ESR dating on Xiashu Loess. J. Nanjing Normal Univ. 16, 86–91 (in Chinese with English abstract).
Li, X.S., Yang, D.Y., Lu, H.Y., 2001. Grain-size features and genesis of the Xiashu loess in Zhenjiang. Mar. Geol. Quatern. Geol. 21, 25–232 (in Chinese with English abstract).
Li, X.S., Yang, D.Y., Lu, H.Y., Han, H.Y., 1997. The grain-size features of Quaternary aeolian-dust deposition sequence in south Anhui and their significance. Mar. Geol. Quat. Geol. 17, 73–81 (in Chinese with English abstract).
Lisiecki, L.E., Raymo, M.E., 2005. A Pliocene-Pleistocene stack of 57 globally distributed benthic $\delta^{18}O$ records. Paleoceanography 20, 1–16.
Liu, C.C., Deng, C.L., 2014. The effect of weathering on the grain-size distribution of red soils in south-eastern China and its climatic implications. J. Asian Earth Sci. 94, 94–104.
Liu, F., Li, G.J., Chen, J., 2014. U-Pb ages of zircon grains reveal a proximal dust source of the Xiashu loess, Lower Yangtze River region, China. Chin. Sci. Bull. 59, 2391–2395.
Liu, J.F., Murray, A.S., Buylaert, J.P., Jain, M., Chen, J., Lu, Y.C., 2016. Stability of fine-grained TT-OSL and post-IR IRSL signals from a c. 1 Ma sequence of aeolian and lacustrine deposits from the Nihewan Basin (northern China). Boreas 45, 703–714.
Liu, T.S., 1985. Loess and the Environment, 65 pp (in Chinese).
Liu, T.S., Ding, Z.L., 1998. Chinese loess and the paleomonsoon. Annu. Rev. Earth Planet. Sci. 26, 111–145.
Lu, H.Y., Stevens, T., Yi, S.W., Sun, X.F., 2006. An erosional hiatus in Chinese loess sequences revealed by closely spaced optical dating. Chin. Sci. Bull. 51, 2253–2259.
Lu, H.Y., Zhang, H.Y., Wang, S.J., Richard, C., Zhao, C.F., Stevens, T., Zhao, J., 2007. A preliminary survey on loess deposit in Eastern Qinling Mountains (Central China) and its implication for estimating age of the Pleistocene lithic artefacts. Quatern. Sci. 27, 559–567 (In Chinese with English abstract).
Lu, H.Y., Wang, X.Y., Li, L.P., 2010. Aeolian sediment evidence that global cooling has driven late Cenozoic stepwise aridification in central Asia. In: Clift, P.D., Tada, R., Zheng, H. (Eds.), Monsoon Evolution and Tectonics-climate Linkage in Asia. Geol. Soc. London Spec. Publ., vol. 342, pp. 29–44.
Lu, H.Y., Sun, X.F., Wang, S.J., Richard, C., Zhang, H.Y., Yi, S.W., Ma, X.L., Wei, M., Yang, Z.Y., 2011. Ages for hominin occupation in Lushi Basin, middle of South Luo River, central China. J. Hum. Evol. 60, 612–617.
Lu, Y.C., Wang, X.L., Wintle, A.G., 2007. A new OSL chronology for dust accumulation in the last 130,000 years for the Chinese Loess Plateau. Quatern. Res. 67, 152–160.
Mejdahl, V., 1987. Internal radioactivity in quartz and feldspar grains. Ancient TL 5, 10–17.
Murray, A.S., Schmidt, E.D., Stevens, T., Buylaert, J.P., Marković, S.B., Tsukamoto, S., Frechen, M., 2014. Dating Middle Pleistocene loess from Stari Slankamen (Vojvodina, Serbia) – limitations imposed by the saturation behaviour of an elevated temperature IRSL signal. CATENA 117, 34–42.
Murray, A.S., 1996. Developments in optically stimulated luminescence and phototransferred thermoluminescence dating of young sediments: application to a 2000-year sequence of flood deposits. Geochim. Cosmochim. Acta 60, 565–576.
Murray, A.S., Thomsen, K.J., Masuda, N., Buylaert, J.P., Jain, M., 2012. Identifying well-bleached quartz using the different bleaching rates of quartz and feldspar luminescence signals. Radiat. Meas. 47, 688–695.
Murray, A.S., Wintle, A.G., 2000. Luminescence dating of quartz using an improved single aliquot regenerative dose protocol. Radiat. Meas. 32, 57–73.
Murray, A.S., Wintle, A.G., 2003. The single aliquot regenerative dose protocol: potential for improvements in reliability. Radiat. Meas. 37, 377–381.
Pan, B.T., Li, J.J., Cheng, F.H., 1995. Qinghai-Tibetan Plateau: a driver and amplifier of global climatic changes. J. Lanzhou Univ. 31, 120–128 (in Chinese with English abstract).
Prescott, J.R., Hutton, J.T., 1994. Cosmic ray contributions to dose rates for luminescence and ESR dating: large depths and long-term time variations. Radiat. Meas. 23, 497–500.
Qiao, Y.S., Guo, Z.T., Hao, Q.Z., Wu, W.X., Jiang, W.Y., Yuan, B.Y., Zhang, Z.S., Wei, J.J., Zhao, H., 2003. Loess-soil sequences in southern Anhui Province: magnetostratigraphy and paleoclimatic significance. Chin. Sci. Bull. 48, 2088–2093.
Qiao, Y.S., Hao, Q.Z., Peng, S.S., Wang, Y., Li, J.W., Liu, Z.X., 2011. Geochemical characteristics of the eolian deposits in southern China, and their implications for provenance and weathering intensity. Palaeogeogr. Palaeoclimatol. Palaeoecol. 308, 513–523.
Reimann, T., Tsukamoto, S., Naumann, M., Frechen, M., 2011. The potential of using K-rich feldspars for optical dating of young coastal sediments – A test case from Darss-Zingst peninsula (southern Baltic Sea coast). Quat. Geochronol. 6, 207–222.
Reimann, T., Tsukamoto, S., 2012. Dating the recent past (< 500 years) by post-IR IRSL feldspar e examples from the North Sea and Baltic Sea coast. Quat. Geochronol. 10, 180–187.
Roberts, H.M., 2008. The development and application of luminescence dating to loess deposits: a perspective on the past, present and future. Boreas 37, 483–507.
Singarayer, J.S., Bailey, R.M., 2003. Further investigations of the quartz optically stimulated luminescence components using linear modulation. Radiat. Meas. 37, 451–458.
Sohbati, R., Murray, A.S., Buylaert, J.P., Ortuño, M., Cunha, P.P., Masana, E., 2012. Luminescence dating of Pleistocene alluvial sediments affected by the Alhama de Murcia fault (eastern Betics, Spain) – a comparison between OSL, IRSL and post-IR IRSL ages. Boreas 41, 250–262.
Spooner, N.A., 1994. The anomalous fading of infrared-stimulated luminescence from feldspars. Radiat. Meas. 23, 625–632.
Stevens, T., Armitage, S.J., Lu, H.Y., Thomas, D.S.G., 2006. Sedimentation and diagenesis of Chinese loess: implications for the preservation of continuous, high-resolution climate records. Geology 34, 849–852.
Stevens, T., Marković, S.B., Zech, M., Sümegi, P., 2011. Dust deposition and climate in the Carpathian Basin over an independently dated last glacial-interglacial cycle. Quatern. Sci. Rev. 30, 662–681.
Sun, X.F., Lu, H.Y., Wang, S.J., Yi, S.W., 2012. Ages of Liangshan Paleolithic sites in Hanzhong Basin, central China. Quat. Geochronol. 10, 380–386.
Sun, J.M., Yin, G.M., Ding, Z.L., Liu, T.S., Chen, J., 1998. Thermoluminescence

chronology of sand profiles in the mu us desert, China. Palaeogeogr. Palaeoclimatol. Palaeoecol. 144, 225–233.
Sun, J.M., Ding, Z.L., 1998. Deposits and soils of the past 130,000 years at the Desert-Loess Transition in northern China. Quatern. Res. 50, 148–156.
Thiel, C., Buylaert, J.P., Murray, A.S., Terhorst, B., Hofer, I., Tsukamoto, S., Frechen, M., 2011. Luminescence dating of the Stratzing loess profile (Austria) – testing the potential of an elevated temperature post-IR IRSL protocol. Quatern. Int. 234, 23–31.
Thomsen, K.J., Murray, A.S., Jain, M., Botter-Jensen, L., 2008. Laboratory fading rates of various luminescence signals from feldspar-rich sediment extracts. Radiat. Meas. 43, 1474–1486.
Vandenberghe, D., De Corte, F., Buylaert, J.P., Kucera, J., Van den Haute, P., 2008. On the internal radioactivity in quartz. Radiat. Meas. 43, 771–775.
Wallinga, J., Murray, A.S., Wintle, A.G., 2000. The single-aliquot regenerative-dose (SAR) protocol applied to coarse-grain feldspar. Radiat. Meas. 32, 529–533.
Wang, X.Y., Lu, H.Y., Zhang, H.Z., Wu, J., Hou, X.X., Fu, F., Geng, J.Y., 2018. Distribution, provenance, and onset of the Xiashu Loess in Southeast China with paleoclimatic implications. J. Asian Earth Sci. http://dx.doi.org/10.1016/j.jseaes.2017.11.022. (in press).
Watanuki, T., Murray, A.S., Tsukamoto, S., 2003. A comparison of OSL ages derived from silt-sized quartz and polymineral grains from Chinese loess. Quatern. Sci. Rev. 22, 991–997.
Watanuki, T., Tsukamoto, S., 2001. A comparison of GLSL, IRSL and TL dating methods using loess deposits from Japan and China. Quatern. Sci. Rev. 20, 847–851.
Wintle, A.G., 1973. Anomalous fading of thermoluminescence in mineral samples. Nature 245, 143–144.
Wintle, A.G., Murray, A.S., 2006. A review of quartz optically stimulated luminescence characteristics and their relevance in single aliquot regeneration dating protocols. Radiat. Meas. 41, 369–391.
Wu, B.Y., 1985. Studies on the sedimentological characteristics of Xiashu Loess in Nanjing. Mar. Geol. Quat. Geol. 5, 113–121 (in Chinese with English abstract).
Wu, S.G., Chen, Y.Y., Yang, D.Y., 1992. A preliminary study on the “Xiashu” clay in Zhenjiang, Jiangsu. In: Liu, T.S., An, Z.S. (Eds.), Loess, Quaternary Geology and Global Change, III. Science Press, Beijing (in Chinese).
Xia, Y.F., Wang, Y.J., Chen, J., 1999. An important stratigraphic boundary in dust accumulation, south China: evidence from magnetic susceptibility. Chin. Sci. Bull. 44, 189–192.
Yang, D.Y., 1991. The Quaternary dust accumulation in East China and monsoon change. Quatern. Sci. 4, 354–359 (in Chinese with English abstract).
Yang, S.Y., Li, C.X., Li, X.S., Wang, A.P., 2001. Geochemical in records of chemical weathering of the Xiashu Loess the lower reaches of the Changjiang River. Geochemic 30, 402–406 (in Chinese with English abstract).
Yi, S.W., Buylaert, J.P., Murray, A.S., Thiel, C., Zeng, L., Lu, H.Y., 2015. High resolution OSL and post-IR IRSL dating of the last interglacial–glacial cycle at the Sanbahuo loess site (northeastern China). Quat. Geochronol. 30, 200–206.
Yi, S.W., Buylaert, J.P., Murray, A.S., Lu, H.Y., Thiel, C., Zeng, L., 2016. A detailed post-IR IRSL dating study of the Niuyangzigou loess site in northeastern China. Boreas 45, 644–657.
Yi, S.W., Lu, H.Y., Stevens, T., 2012. SAR TT-OSL dating of the loess deposits in the Horqin Dunefield (northeastern China). Quat. Geochronol. 10, 56–61.
Zhang, W.G., Yu, L.Z., Lu, M., Zheng, X.M., Shi, Y.X., 2007. Magnetic properties and geochemistry of the Xiashu Loess in the present subtropical area of China, and their implications for pedogenic intensity. Earth Planet. Sci. Lett. 260, 86–97.
Zhao, H., Li, S.H., 2005. Internal dose rate to K-feldspar grains from radioactive elements other than potassium. Radiat. Meas. 40, 84–93.